Numerical Investigation on the Interior Wind Noise of a Passenger Car

Liu Ying-jie, Lu Wen-bo, Peng Cheng-jian

***Abstract*—**With the development of the automotive technology and electric vehicle, the contribution of the wind noise on the interior noise becomes the main source of noise. The main transfer path which the exterior excitation is transmitted through is the greenhouse panels and side windows. Simulating the wind noise transmitted into the vehicle accurately in the early development stage can be very challenging. The basic methodologies of this study were based on the Lighthill analogy; the exterior flow field around a passenger car was computed using unsteady Computational Fluid Dynamics (CFD) firstly and then a Finite Element Method (FEM) was used to compute the interior acoustic response. The major findings of this study include: 1) The Sound Pressure Level (SPL) response at driver's ear locations is mainly induced by the turbulence pressure fluctuation; 2) Peaks were found over the full frequency range. It is found that the methodology used in this study could predict the interior wind noise induced by the exterior aerodynamic excitation in industry.

***Keywords*—**Wind noise, computational fluid dynamics, finite element method, passenger car.

I. Introduction

THE interior noise of the highway speed vehicle due to the exterior airflow has always been a source of concern for consumers and automotive manufactures. With the development of quieter electric and hybrid vehicles, the interior wind noise is becoming increasingly important because the other noise sources have disappeared or have been reduced dramatically. The aeroacoustic loads on the exterior transmit into the cabin through many paths (e.g., greenhouse and underbody). The wind noise transmitted through the greenhouse and side windows often dominate the interior wind noise level [1], [2]. Nowadays, thinner panels have been widely used as a way of vehicle weight reduction, thereby increasing the severity of structural noise transmission problem. In fact, in the last decades, addressing the noise transmitted through the greenhouse has arouse a great deal of attention, especially the noise generated by the side mirror [3], [4].

The influence of the wind noise on the overall noise level inside the cabin could be evaluated by wind tunnel experiment. However, due to the high cost and pressures on the product development cycle, the numerical simulation can be an alternative in the early stages of the design process. Previous researches have presented that the accuracy of the numerical simulation is enough to compute the noise source and the noise transmission from the vehicle body into the cabin. For instance, Crouse et al. [1] used the Lattice-Boltzmann Method (LBM) combined with a two-equation renormalization group (RNG) turbulence model to analyze the wind noise sources in passenger car. The results showed that the fluctuating pressure in the underbody region dominated at 200 Hz 1/3 octave band compared with other frequencies. For noise transmission, the CFD combined with the Statistical Energy Analysis (SEA) has been developed to predict the wind noise propagated from the greenhouse into the cabin [5], [6]. However, this approach had a limited accuracy to resolve the issue related to the low frequency. Dobrzynski [7] investigated the contribution of interior noise levels from the different parts of the car body, and research showed that the contribution from the aerodynamic noise sources dominated the low frequency regime. It is, therefore, necessary to calculate the low frequency noise accurately for predicting the impact of wind induced noise in the cabin. Moreover, the CFD/FEM approach has been successfully used to deal with side windows and windshield wind noise prediction [8], [9]. Therefore, in current research, the CFD/FEM approach is extended to handle the wind noise transmitted through the green house panel. The exterior turbulent flow field was first captured by a transient CFD analysis based on Large Eddy Simulation. Then noise transmission and propagation were conducted using a specific finite element aero-vibro-acoustic computational strategy. Unlike the noise from engine or tire, the wind noise has two different types of excitation contributions, which will be described in the next section. Two load cases corresponding to the acoustic and turbulent components have been analyzed.

Liu Ying-jie is with the China Faw Group Co. Ltd, State Key Laboratory of Comprehensive Technology on Automobile Vibration and Noise & Safety control, Changchun 13000, China.
Lu Wen-bo is with the Shanghai Hikey-Sheenray Information Technology Co. Ltd., Shanghai 200235, China (e-mail: wenbo326@163.com).
Peng Cheng-jian is with the School of automotive engineering, Wuhan University of Technology, Wuhan 430070, China.

II. Exterior Noise Source Computation

A. Geometrical Model

In current research, the geometrical model of the passenger car is shown in Fig. 1. In order to save computing resources, some of the vehicle parts which have little effect on the flow field have been simplified, such as the door handle, wiper, antenna, grille were deleted.

B. Numerical Method

The interior wind noise is caused by the unsteady pressure fluctuations on the greenhouse panels. These noise sources mostly originate from the turbulent boundary layers, turbulent flow separations and natural turbulence inherent in the free-stream as the vehicle travels in the fluid medium. As a result, the premise of the interior wind noise computation is to get the exterior excitation. Therefore, an accurate calculation of the exterior flow fields around the model is the key point. Recent development of CFD provides a powerful tool for the prediction of unsteady flow field.

Fig. 1 Geometrical model of a passenger car

In current research, an incompressible flow field was assumed. The filtered Navier-Stokes equations was used to express the resolved field parameters as,

$$\frac{\partial \tilde{u}_i}{\partial x_i} = 0 \tag{1a}$$

$$\frac{\partial \tilde{u}_i}{\partial t} + \tilde{u}_j \frac{\partial \tilde{u}_i}{\partial x_j} = -\frac{1}{\rho}\frac{\partial \tilde{p}}{\partial x_i} + \nu \frac{\partial^2 \tilde{u}_i}{\partial x_j \partial x_j} - \frac{1}{\rho}\frac{\partial \tau_{ij}}{\partial x_j} \tag{1b}$$

where ρ and υ were the density and kinematic viscosity of air, respectively. The tensor notations were used in (1a) and (1b) where i, j = 1, 2, 3 represent the respective parameters in the directions along the co-ordinate axes.

For aeroacoustics, Lighthill [10] derived the acoustic wave equation from the N-S equations, which revealed the mechanism of sound due to the airflow.

$$\frac{\partial^2 \rho'}{\partial t^2} - c_0^2 \nabla^2 \rho' = \frac{\partial^2 T_{ij}}{\partial x_i \partial x_j} \tag{2a}$$

$$T_{ij} = \rho u_i u_j + \delta_{ij}[(p - p_0) - c_0^2(\rho - \rho_0)] \tag{2b}$$

where T_{ij} is the Lighthill stress tensor, if the right side of the equation is treated as a sound source, the solution of (2) can be obtained by the classical acoustic method. Among them, the stress tensor in the sound source can be calculated numerically.

C. Grid Generation

The computational domain in this paper is shown in Fig. 2. The calculated domain width is seven times the width of the car (about three times each), the height is five times as high as the car model, and the length is 11 times as long as the model.

For mesh, the tetrahedron grid has the advantages of convenient adjustment of the size, number of regional grids and strong adaptability to geometry. Due to the need of aeroacoustic calculation, the mesh generation meets not only the CFD calculation accuracy requirements but also the acoustic calculation requirements. The aerodynamic noise in current research is calculated in the frequency range of 0-500 Hz. The maximum length of the acoustic grid is 113.33 mm. The size of the car surface grid for CFD is 20 mm, and the surface mesh is shown in Fig. 3.

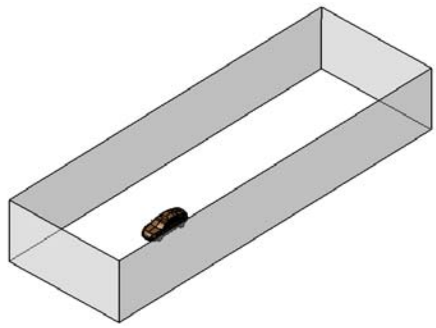

Fig. 2 Computational domain

Fig. 3 Body surface mesh

For the boundary layer grid, the thickness of the first layer was set to 0.2 mm, the growth rate was 1.2 and a total of 5 layers were obtained (see Fig. 4).

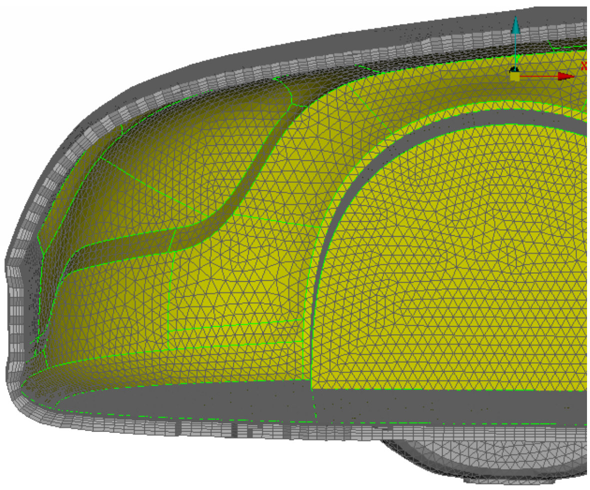

Fig. 4 Boundary layer grid

In order to conveniently control the number of grids, three density boxes are provided for controlling the grid size and growth rate in different grid areas, Fig. 5 shows the position of the density boxes.

D. Boundary Conditions and Scheme Setup

The boundary conditions are shown in Table I. The steady-state solver settings are shown in Table II.

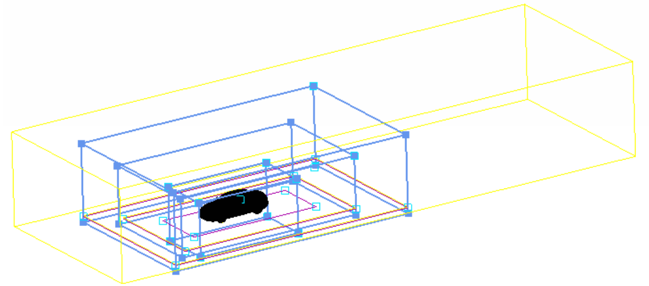

Fig. 5 The location of density boxes

TABLE I
BOUNDARY CONDITIONS

Position	Description
Entrance	Speed entrance: 30 m / s
Export	Pressure outlet: 0 Pa
Body surface + ground	No slip Static wall
other	Symmetrical wall

TABLE II
STEADY STATE SOLVER SETTINGS

Setting item	Settings
Solver	Pressure Based
Time	Steady
Pressure speed coupling	SIMPLE
Pressure Discrete	2nd order
Momentum Discrete	2nd order up wind
Energy Discrete	2nd order up wind

In the steady-state calculation, the aerodynamic drag coefficient and the average pressure on the left front and rear left windows were monitored to verify the grid independence. The comparisons between different grid strategies are shown in Table III. The time step for the unsteady computation was set to 4e-04s. The total calculation time is 1.2s.

TABLE III
COMPARISONS BETWEEN DIFFERENT GRID STRATEGIES

Number of grids	Cd	Average pressure on left front side window (Pa)	Average pressure on left rear window (Pa)
7.79 million	0.266	-181.44	-129.54
12.6 million	0.269	-181.77	-129.49
17.2 million	0.270	-180.67	-127.88

Since the error between three cases is less than 2%, taking into account the relationship between acoustic calculation accuracy and computational resources, the grid number of 12.6 million was selected.

E. Computational Results of Exterior Flow Field

As shown in Fig. 6, because of the blockage effect, the airflow is accelerated around the rear view mirrors, and the unstable shear layer, which will induce vortex shedding, is produced. As a result, the turbulent pressure pulsation is induced on the side windows.

The side window pressure values shown in Fig. 7 revealed that the vortex sheds from the rear of the A-pillar and the rear-view mirror and acts on the front side window, and then continues to develop and act on the rear side window.

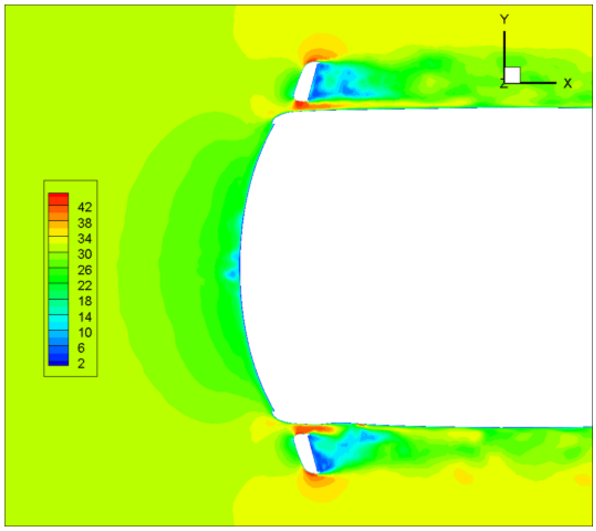

Fig. 6 Velocity distribution along the horizontal section

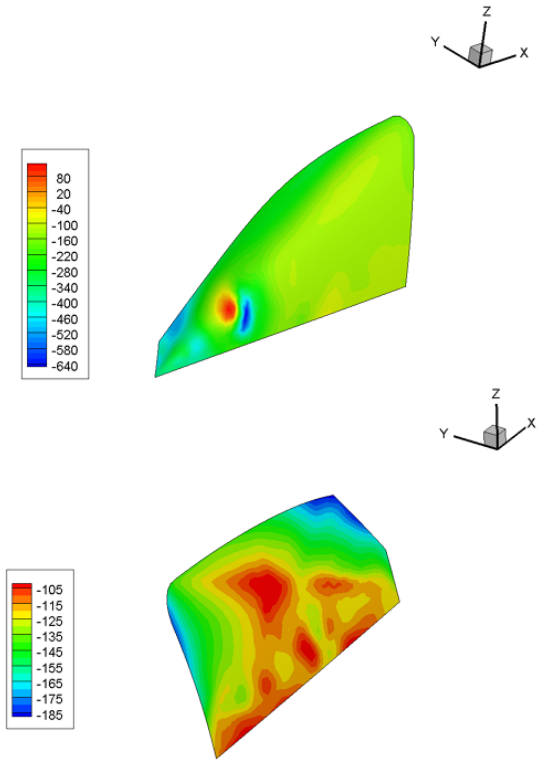

Fig. 7 Pressure distribution on the left side window

F. Vibro- Acoustic Model

The vibra-acoustic model (Fig. 8) was set up to compute the noise transmission into the cabin. The model includes the driver, steering wheel, seat, center console and dashboard. The cabin is meshed with tetrahedron and the number of grids is 370,000.

G.Aero-Acoustic Model

For the aero-acoustic model, a noise source region in which the acoustic wave propagates (Fig. 7) was set up around the vehicle body and modeled with physical finite fluid component. Moreover, an infinite element was placed at the outer surface of the acoustic finite element region to model a free field.

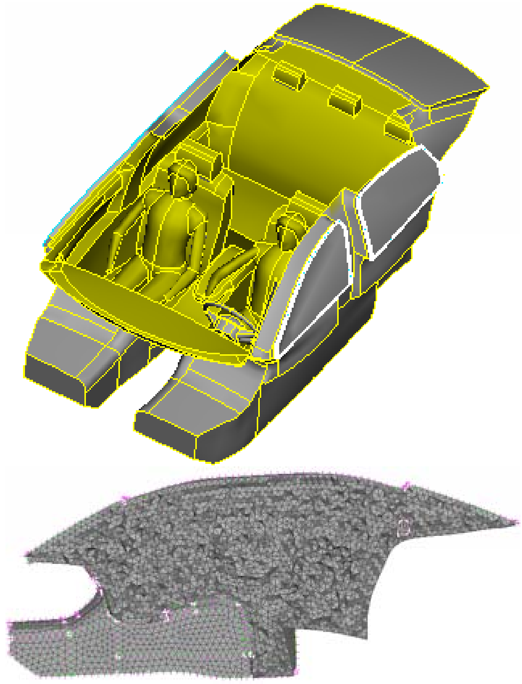

Fig. 8 Vibra-acoustic model

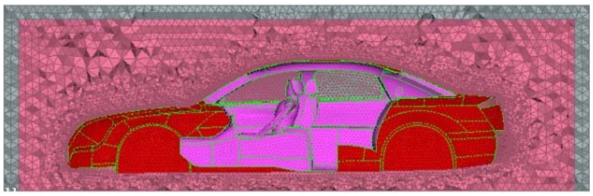

Fig. 9 Aero-acoustic model

H. Acoustic Computation Results

The monitoring points are arranged at the left and right ear of the driver and left driver to monitor the sound pressure inside the cabin, as shown in Fig. 10.

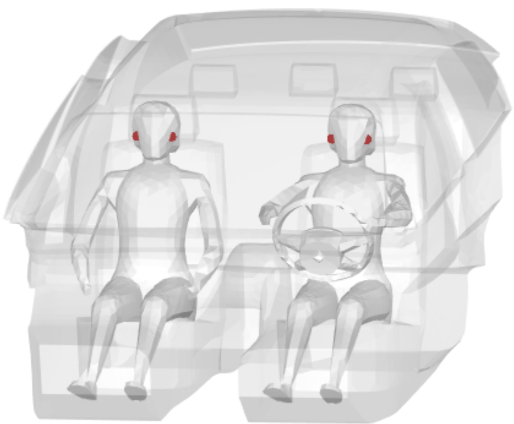

Fig. 10 Monitoring point location

Taking the monitoring point on the left ear of the driver as an example, the result of the contribution of the noise caused by the turbulence and the aerodynamic noise is shown in Fig. 11. It can be seen that, above 200 Hz, the interior noise caused by the turbulence pressure on the side window is larger than the aerodynamic noise outside the car, while below 200 Hz, the former is lower than the latter. In addition, the sound pressure at the monitoring point has obvious peak value, the highest peak is located at 260 Hz, and the sound pressure intensity is up to 58 dB. The contribution of noise caused by turbulent fluctuation and the contribution of aerodynamic noise is similar.

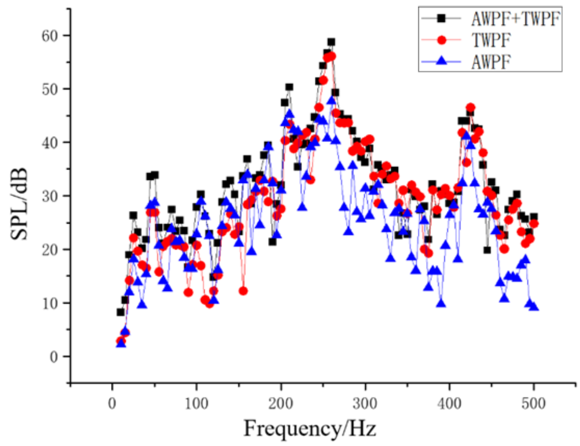

Fig. 11 SPL at the driver left ear

The contribution of different noise source to the interior noise plotted in Fig. 12 shows that the noise contribution from the left front side window is larger than the contribution from the left rear side window at most frequencies.

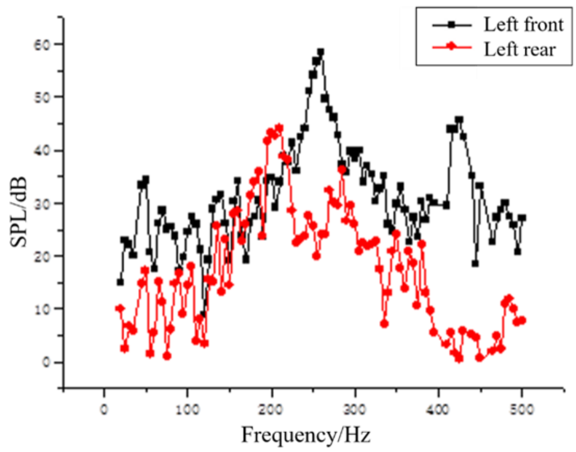

Fig. 12 Comparison between the contributions of different noise source to the interior noise

Fig. 13 showed the sound pressure inside the cabin at some peak frequencies. It can be seen that the noise level near the window is relatively higher. The sound pressure distribution has different characteristics under different frequencies. Around 200 Hz, the SPL at the rear is higher than the front, but at 260 Hz and 450 Hz, the front is higher that rear.

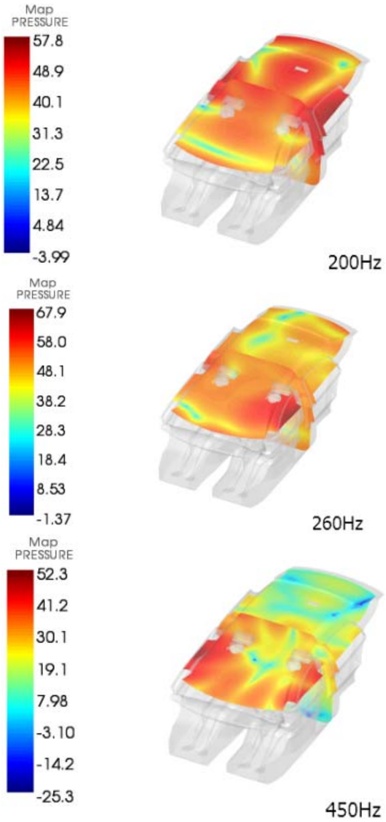

Fig. 13 Sound pressure inside cabin

III. Conclusion

In this paper, an explicit approach coupling CFD and FEM via aero-vibro acoustic strategy was used to handle the wind noise transmitted into the cabin. The turbulent wall pressure fluctuations as well as the acoustic wall pressure fluctuations (after the noise sources calculation in the airflow) on the side windows were computed with the CFD results firstly. Then the SPL inside the cabin was captured based on the vibro-acoustic calculation with a FEM cabin model. The final results revealed that the SPL at driver's ear due to the turbulence pressure on the side window was little higher than that owing to the aerodynamic noise source above 200 Hz. The SPL discrepancies between driver and passengers were not so prominent. Furthermore, peaks are found over the full frequency range.

Acknowledgment

The research was supported by the Open fund of State Key Laboratory of Comprehensive Technology on Automobile Vibration and Noise&Safety control (Grant No. 1803J-W65-GNZX-2018-0215) and National Natural Science Foundation of China (Grant No. 51775395).

References

[1] Crouse, B., Freed, D., Senthooran, S., Ullrich, F., Fertl, C., "Analysis of Underbody Windnoise Sources on a Production Vehicle using a Lattice Boltzmann Scheme," SAE Technical Paper 2007-01-2400, 2007.
[2] Moron, P., Hazir, A., Crouse, B., Powell, R., Neuhierl, B., Wiedemann, J., "Hybrid Technique for Underbody Noise Transmission of Wind Noise," SAE Technical Paper 2011-01-1700, 2011.
[3] Wang, Y., Gu, Z., Li, W., Lin, X., Les, A., "Evaluation of Aerodynamic Noise Generation by a Generic Side Mirror," World Academy of Science, Engineering and Technology 61 2010.
[4] Yao, H., L, Davidson., "Generation of interior cavity noise due to window vibration excited by turbulent flows past a generic side-view mirror," Physics of Fluids 30, 036104 (2018).
[5] Moron, P., Powell, R., Freed, D., Perot, F., Crouse, B., Neuhierl, B., Ullrich, F., Holl, M., Waibl, A., Fertl, C., "A CFD/SEA Approach for Prediction of Vehicle Interior Noise due to Wind Noise," SAE Technical Paper 2009-01-2203, 2009.
[6] Lepley, D., Graf, A., Powell, R., and Senthooran, S., "A Computational Approach to Evaluate the Vehicle Interior Noise from Greenhouse Wind Noise Sources," SAE Technical Paper 2010-01-0285, 2010.
[7] Dobrzynski W (1986) Wind induced interior and far field radiated exterior noise from automobiles. In vehicle aerodynamics, Von Karman Inst. for Fluid Dynamics lecture series, 1986.
[8] Van Herpe, F., D'Udekem, D., Jacqmot, J., and Kouzaiha, R., "Vibro-Acoustic Simulation of Side Windows and Windshield Excited by Realistic CFD Turbulent Flows Including Car Cavity," SAE Technical Paper 2012-01-1521, 2012.
[9] Schell, A. and Cotoni, V., "Prediction of Interior Noise in a Sedan Due to Exterior Flow," SAE Int. J. Passeng. Cars - Mech. Syst. 8(3): 1090-1096, 2015.
[10] Lighthill M J. On Sound Generated Aerodynamically I. General Theory (J). Proceedings of the Royal Society of London. Series A. Mathematical and Physical Sciences, 1952,211(1107):564.